EES Solar

PAPER

View Article Online
View Journal

Cite this: DOI: 10.1039/d6el00021e

Modelling and predicting real-world lifetime of perovskite–silicon tandem solar cells using advanced energy yield models with degradation kinetics

Seyedamir Orooji, [ab] Felix Laufer, [ab] Sam Teale,[c] Henry Snaith [c] and Ulrich W. Paetzold *[ab]

Long-term stability of the perovskite top cell remains a hurdle to commercializing perovskite–silicon tandem (PST) solar cells. While accelerated tests provide valuable insights into degradation kinetics, they fail in predicting real-world degradation behavior. Keeping stressors constant, accelerated tests neglect dynamic conditions in actual operational environments, like diurnal and seasonal temperature and irradiance variability. We address this challenge by integrating a degradation function into our energy yield (EY) modelling software which integrates degradation in collection efficiency (and thus photocurrent) over time due to light and heat exposure, bridging the gap between accelerated testing and in real-world stability assessment. By linking the EY model to measurable material parameters like activation energy governing degradation pathways, this approach enables physically grounded degradation modelling. Based on degradation observed under accelerated tests, the model predicts PST operational lifetimes in diverse climates, highlighting the substantial discrepancy between lifetimes measured under accelerated testing and real-world locations. Applied to a PST solar cell, we show that an operational lifetime ($T_{90,Agg}$) of about 1400 h under ISOS-L2 (1 Sun, 85 °C), translates to several months in-field (about 26 months in arid Phoenix and 42 months in temperate Seattle), demonstrating strong climate dependence. We also provide a practical mapping from ISOS-L2 to real-world lifetimes and estimate the minimum stability threshold needed for deployment as around 4000 h $T_{90,Agg}$ under ISOS-L2, translating to more than 5 years of operation across the investigated locations. After device-specific parameterization from appropriate aging tests, this device-agnostic framework allows stability-aware EY modelling to predict real-world degradation.

Received 9th February 2026
Accepted 19th April 2026

DOI: 10.1039/d6el00021e

rsc.li/EESSolar

Broader context

Perovskite–silicon tandem solar cells promise higher efficiencies than conventional photovoltaics, but their commercial deployment is limited by the long-term stability of the perovskite top cell. Device lifetimes are typically assessed using accelerated aging tests under constant stress conditions, yet real-world operation involves continuously varying temperature and solar irradiance. This mismatch makes it difficult to translate laboratory stability metrics into meaningful predictions of field performance. In this work, we bridge this gap by integrating physically grounded degradation modelling into energy yield simulations, linking accelerated test results to realistic climate conditions. By connecting degradation rates to measurable material properties, this approach enables climate-specific lifetime predictions and reveals large discrepancies between accelerated and real-world stability. Our framework provides a practical pathway for translating laboratory aging tests into deployment-relevant lifetime targets, supporting more reliable stability assessment and design of next-generation tandem solar cells.

1. Introduction

Perovskite–silicon tandem (PST) solar cells are advancing rapidly, with certified power-conversion efficiencies (PCEs) approaching 35%,[1–3] well beyond the practical limits of single-junction silicon photovoltaics (PV).[4] Despite these remarkable advances, the insufficient long-term stability of the perovskite top cell remains a barrier to large-scale industrial deployment of PST solar cells.[5–15] The performance loss in PST devices is largely

[a]Institute of Microstructure Technology, Karlsruhe Institute of Technology, Hermann-von-Helmholtz-Platz 1, 76344 Eggenstein-Leopoldshafen, Germany. E-mail: ulrich.paetzold@kit.edu

[b]Light Technology Institute, Karlsruhe Institute of Technology, Engesserstrasse 13, 76131 Karlsruhe, Germany

[c]Department of Physics, University of Oxford, Clarendon Laboratory, Parks Road, Oxford, OX1 3PU, UK

attributed to various extrinsic and intrinsic degradation mechanisms triggered by elevated temperature, light exposure, humidity, and voltage bias in the perovskite top cell.[16–25] To replicate years of in-field degradation within practical laboratory timescales, accelerated testing protocols have been devised that expose PST devices to elevated stress levels, thereby induce faster degradation.[26] The ISOS (International Summit on Organic Photovoltaic Stability) protocols standardized these tests to enable comparison across different studies. ISOS-L (light-soaking) probes degradation under continuous illumination, whereas ISOS-D (dark storage) evaluates stability against constant ambient stressors such as temperature and humidity. Complementary protocols (*e.g.*, ISOS-T, ISOS-LC, ISOS-LT) introduce cyclic variations in temperature, irradiance, and humidity to better approximate real operating environments, which can induce different degradation pathways than constant-stress conditions.[27] Despite providing valuable insights, these accelerated tests do not mimic real-world operation sufficiently as they overlook environmental variations that vary diurnally and seasonally in temperature and irradiance. As a result, in-lab lifetimes are only tangentially related to real-world field performance. We address this gap by integrating a novel degradation function into our in-house open-source energy yield (EY) modelling software, EYCalc,[28] which allows predicting PST lifetimes across a range of geographical locations and climates based on degradation trends observed under accelerated tests conditions. In the laboratory, PST performance is typically characterized by measuring PCE under standard test conditions (STC: 1000 W m^{-1} AM1.5G irradiance at 25 °C). While PCE provides a convenient reference, it represents only a single operating point and does not capture real-world performance. In contrast, analysing the EY of PSTs takes into account a wide range of environmental factors, including fluctuations in irradiance, spectral shifts, temperature variations, cloud cover, and varying incident angles. Integrating the influence of both temperature and light stressors, this study introduces a degradation model that combines combined thermal and photo-induced degradation. The model links degradation to measurable kinetics and outputs operational lifetime, defined here as $T_{90,Agg}$, the time at which the aggregated power output of the degraded cell decreases to 90% of that of the non-degraded cell. Conventionally, T_{90} is defined using the instantaneous power ratio P_t/P_0, where P_t reaches 90% of the initial power P_0. However, to enable a fair comparison between accelerated test results and real-world operation, where power output varies hourly, this study instead employs an aggregated power ratio. To implement the temperature dependence of the degradation, the widely used Arrhenius expression[29–32] is utilized as it captures the exponential dependence of degradation rates against temperature.[29,33] To introduce the light-intensity dependence of the degradation process, a power-law relationship is employed capturing the sublinear relationship between light-intensity and degradation described by Siegler *et al.*[34] Investigating the impact of both stressors, this study uses the product of the Arrhenius and power-law expressions to capture the combined effect of thermal and photo-induced degradation.[35] Based on this improved EY model, we demonstrate how degradation trends observed under accelerated testing can translate to PST degradation in real-world field deployment. Using a published stability study as a reference for parameterization, our results suggest a substantially longer operational lifetime ($T_{90,Agg}$) for PST solar cells under real-world operating conditions compared to standard accelerated tests. Having confirmed this substantial difference, we determine the ISOS-L2 (85 °C) lifetime required to ensure acceptable operational lifetime in several real-world locations.

2. Methodology

2.1. Modular framework of EYCalc

To improve EY modelling by integrating degradation kinetics, this work builds on our in-house developed, open-access EY modelling software, EYCalc, which is designed to provide EY predictions based on the physical properties of solar cells, their installation parameters, and site-specific irradiation and ambient conditions.[28] A comprehensive description of the software is provided by Schmager *et al.*[36] Here, we provide a brief overview of its modular workflow. EYCalc consists of four modules: irradiance, optics, electrics, and the core EY module (see Fig. 1a). The irradiance module calculates with hourly resolution the direct and diffuse irradiance spectra for various locations in the US and Europe over a year. It processes typical meteorological year (TMY3) data provided by NREL[37] for locations across US and combination of ERA5 and CAMS datasets provided by ECMWF for locations in Europe.[38–41] Then it uses a simplified atmospheric radiative transfer model[42] to compute clear-sky irradiance. A simple cloud model is then used to account for weather effects. The optics module determines the spectrally and angularly resolved reflectance, transmittance, and absorptance for each layer of the stack. These parameters are computed using the transfer-matrix method for thin (optically coherent) layers and a Beer–Lambert law series expansion for thick (optically incoherent) layers. In addition, the module can simulate layer stacks with textured interfaces using geometric ray tracing, as reported by Baker–Finch and McIntosh.[43] The module is particularly well suited to model the EY of textured PST solar cells in two-terminal, four-terminal and three-terminal architectures.[44–47] The EY module calculates the hourly photogenerated current density (J_G) in the absorber layers based on the computed irradiance and optical properties of the layers while also considering the solar cell's orientation. The electrics module generates the temperature-dependent current density–voltage (J–V) characteristics of the solar cell based on the output of the EY module combined with equivalent circuit parameters (diode parameters), including the dark-saturation current density (J_0), collection efficiency (CE), series resistance (R_S), and shunt resistance (R_{Sh}). The tandem device is represented by two diodes, corresponding to the perovskite top cell and the silicon bottom cell. For this process, a precise numerical method or an analytical two-diode model can be used. In this study, we used a precise numerical two-diode model by using LTspice (the baseline device and diode parameters before degradation can be found in Fig. SI1 and Table SI1).[48] Accurate prediction of EY and solar cell lifetime under

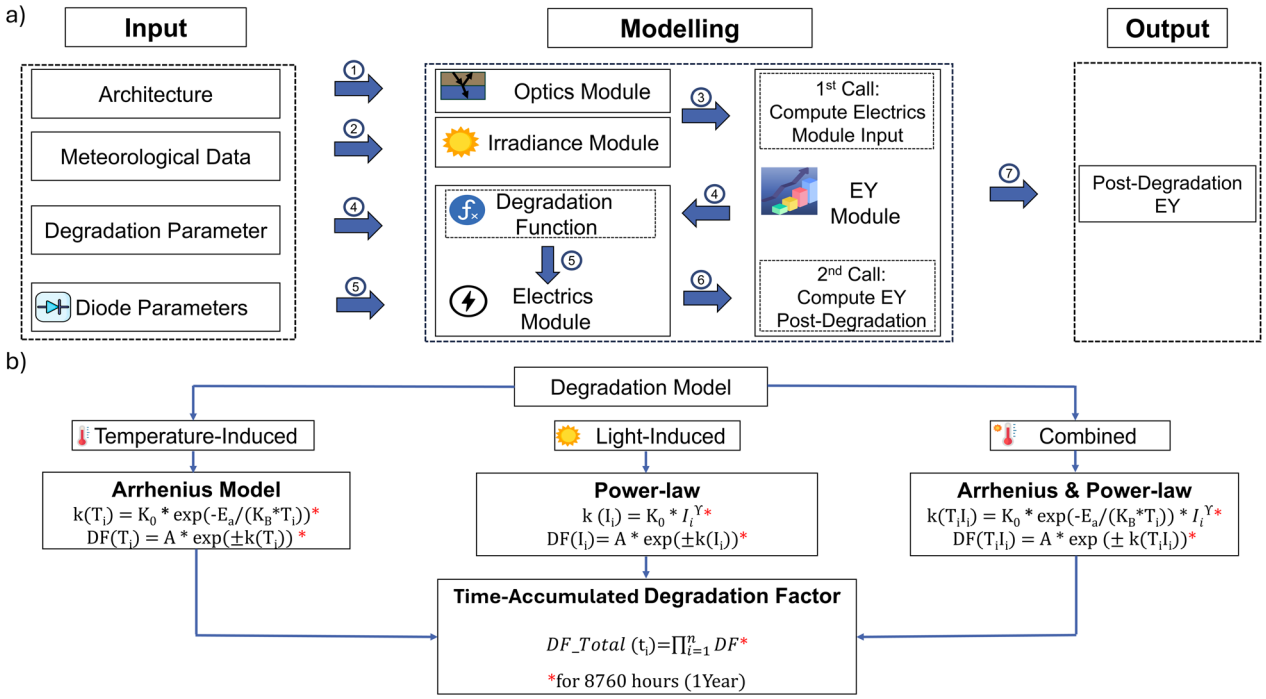

Fig. 1 (a) Modular workflow of EYCalc, incorporating the irradiance, optical, and electrical modules with the degradation function to compute solar cell energy yield under thermal and light-induced stress conditions. (b) Internal workflow of the degradation function within the EY simulation framework. Three degradation models (temperature-induced (Arrhenius), light-induced (power-law), and a combined model) are exemplary shown and used here to compute the hourly degradation rate (k) and degradation factor (DF) over the course of a year. These hourly values are accumulated into a time-dependent degradation factor (DF_total), which are applied to the initial value of diode parameters in the electrics module to generate time-resolved J–V characteristics and compute the final energy yield. Depending on the diode parameter responsible for degradation, the degradation factor DF(T_i) may represent either a decrease (*e.g.*, CE or R_{Sh}) or an increase (*e.g.*, R_S or J_0) in the corresponding parameter.

degradation requires modelling device parameters that evolve with the hourly heat and light conditions observed in the field. This work extends the electrics module with a novel degradation function that considers the time-dependent variation of heat and light, two key degradation stress factors. With this extension, the module determines the J–V characteristics of the solar cell undergoing degradation. The degradation function calculates a time-accumulated degradation factor (DF_total), capturing the evolution of degradation rates over time, which is then applied to the initial value of the diode parameters in the electrical module to produce post-degradation time-resolved J–V characteristics. Finally the EY core module determines the post-degradation annual EY. In this work, degradation is assumed to occur only in the perovskite top cell, while the silicon bottom cell remains stable. Therefore, the parameter DF_total is applied only to the diode parameters of the perovskite top cell.

2.2. Degradation function

The degradation function converts hourly-resolved information on stressors into a cumulative factor that updates diode parameters in the electrics module (see Fig. 1b). It accounts for the time-dependent variation of the two key stressors, heat and light, by supporting three degradation models: (i) temperature-induced, (ii) light-induced, and (iii) combined temperature- and light-induced degradation. To represent degradation driven solely by temperature variation the Arrhenius expression is used in the temperature-induced model. This widely-used model is well-suited for describing thermally activated degradation mechanisms, as it captures the exponential dependence of the degradation rates with cell temperature.[29,33] The light-induced model applies a power-law relation to describe degradation caused exclusively by changes in irradiance. This model has been used previously as it captures the observed sublinear dependence of degradation rate with light-intensity, however, limited data exists on degradation dependence and light intensity. To capture the effects of both stressors, the degradation function multiplies the Arrhenius expression and the power law.[33,35]

As this study focuses on combined temperature- and light-induced degradation modelling, the degradation function combines the Arrhenius expression and the power-law model to capture the effect of temperature and light. We briefly describe the parameters in these two models. The Arrhenius expression describes how temperature accelerates degradation which leads to the temperature dependence of the degradation rates:

$$k(T) = k_0 \times \exp\left(\frac{-E_a}{k_B \times T}\right) \quad (1)$$

Here, $k(T)$ is the degradation rate, k_0 is the pre-exponential factor (dependent on degradation mechanisms and

architecture of the cell),[29] E_a is the activation energy in eV that indicates the sensitivity of degradation to temperature variation, k_B is the Boltzmann constant, and T is the cell temperature in kelvin. To estimate the cell temperature, we use the Nominal Operating Cell Temperature (NOCT) model,[49] assuming a NOCT of 48 °C. Eqn (2) shows how cell temperature is calculated using NOCT model. S is incident insolation in mW cm^{-2}. Our framework is also able to accommodate more complex temperature models.

$$T_{cell} = T_{air} + \frac{NOCT - 20}{80} \times S \quad (2)$$

Light accelerates degradation with a power-law describing the light-intensity dependence of the degradation rates:

$$k(I) = k_0 \times I^{\gamma} \quad (3)$$

In this model, k_0 is the pre-exponential factor, I is the light intensity at each time step (corresponding to the actual light-intensity, including zero values during night-time), and γ is the light exponent, which like k_0 depends on the architecture and the degradation mechanism.

The model describing both temperature- and light-induced degradation multiplies the temperature and light terms to capture the effects of both stressors:

$$k(T, I) = k_0 \times \exp\left(\frac{-E_a}{k_B \times T}\right) \times I^{\gamma} \quad (4)$$

The duration of exposure to stressors also affects the degradation process. Depending on the solar cell architecture and underlying degradation mechanism, the degradation can follow different trends such as linear, exponential, or double-exponential. In our model, this time dependence is represented by the total degradation factor (DF_total), which accounts for the impact of exposure duration on solar cell performance. After computing the total degradation factor (DF_total), we multiply the initial value of the affected diode parameter by DF_total, and the electrics module recomputes the post-degradation J–V characteristics.

For accelerated tests such as ISOS protocols, where both light intensity and temperature remain constant, the total degradation factor over a defined exposure period (*e.g.*, 1000 hours) can be expressed in closed form. For example, if the degradation follows an exponential trend and "t" is the exposure time, the total degradation factor is given by:

$$DF\_total(t) = \exp(-k \times t) \quad (5)$$

where k is the degradation rate.

For real-world locations, temperature and light intensity fluctuate over time. In this case, the model calculates the total degradation factor as the cumulative product of the hourly degradation factors (DF(t)).

$$DF\_total(t) = \prod_{t=1}^{n} DF(t) \quad (6)$$

In this study, degradation is assumed to occur only in the perovskite top cell, while the silicon bottom cell remains unchanged. Accordingly, all parameters discussed in this section (*e.g.*, k_0) are applied only to the perovskite top cell, whereas the parameters of the silicon bottom cell are kept constant. Degradation modelling is performed at the diode parameter level. Through variations in the corresponding diode parameters (*i.e.*, CE, J_0, R_{Sh}, and R_S), we study the impact of degradation on solar cell parameters (*i.e.*, J_{SC}, V_{OC}, FF) and the overall performance of the solar cell. Using this approach, degradation in J_{SC} is studied through a decline in CE, degradation in V_{OC} through an increase in J_0, and degradation in FF through either a decrease in R_{Sh} or an increase in R_S. In our previous study,[50] we provided a comprehensive discussion on the importance of studying degradation at the level of diode parameters. We demonstrated that the impact of degradation on the solar cell performance varies significantly depending on the diode parameter responsible for degradation. Although perovskite solar cells have been shown to partially or even fully recover from degradation during dark periods,[51–54] we do not include this healing process in this study for simplicity. Instead, we assume that degradation occurs only under illumination, and the degradation rate remains unchanged during dark hours.

2.3. References for degradation model parameterization

Realistic lifetime and EY predictions require device-specific degradation kinetics; therefore, we parameterize the model using well-characterized device-specific degradation kinetics, specifically for a PST solar cell, and utilize these parameters for all subsequent simulations. We study the impact of combined temperature- and light-induced degradation, assuming that degradation occurs exclusively in the perovskite top cell, while the silicon bottom cell remains stable for simplicity. For the reference PST solar cell, we use the device reported by Liu *et al.* in,[55] which achieved a PCE of 33.89%. The architecture of the reference cell used in this study, along with the corresponding experimental and simulated baseline electrical and optical parameters, is shown in Fig. SI1. It is a particularly well-suited reference as it provides the largest amount of input parameters required for our modelling among all published record PCEs for PST solar cells over recent years. We parameterize the degradation model by extracting degradation-related parameters (*e.g.*, activation energy, pre-exponential factors) from the paper by Zhao *et al.*,[56] in which the degradation of an inorganic perovskite solar cell was investigated under accelerated tests. While the work reported degradation for devices, with and without a two-dimensional $Cs_2PbI_2CI_2$ capping layer, we focus on the device without the 2D capping layer. This study reported two activation energies, representing fast (0.248 eV) and slow (0.243 eV) degradation processes. In their study, the time evolution of the PCE was fitted using a double-exponential decay function, from which the degradation rate constants for the fast (k_{fast}) and slow (k_{slow}) processes were obtained. These rate constants were then used in the Arrhenius relation to

determine the corresponding activation energies. The PCE decay over time is expressed as:

$$\mathrm{PCE}\ (t) = A_1 \times \exp(-k_{\mathrm{fast}} \times t) + A_2 \times \exp(-k_{\mathrm{slow}} \times t) + B \quad (7)$$

They applied a constant illumination of 1200 W m^{-2} and temperatures of 35, 59, 85, and 110 °C. The values of A_1, A_2, B, k_{fast}, and k_{slow} were obtained by fitting the observed degradation trends to eqn (7). The activation energies were then extracted using the Arrhenius expression. Based on the reported degradation trends in this reference, degradation can be analysed at the level of different diode parameters (*i.e.*, CE, J_0, R_{sh}, and R_{s}). In this study, the degradation factor DF_total is applied to the CE, rather than directly to the PCE (see eqn (8) and (9)), thereby representing degradation in the J_{SC}. CE was selected because variations in this parameter show an intermediate impact on device degradation compared to the stronger influence of R_{Sh} and the weaker influence of R_{S}, as reported in our previous work.[50] Furthermore, only one diode parameter is varied in order to isolate its contribution to the overall degradation, as simultaneously varying multiple parameters would make it difficult to distinguish their individual impacts. Since our study focuses on J_{SC} degradation due to a decline in CE, the time-evolution of CE can be expressed in closed-form for accelerated tests, or by using DF_total parameter for real-world locations where we have temperature and light-intensity fluctuations over time.

For accelerated tests:

$$\mathrm{CE}\ (t) = A_1 \times \exp(-k_{\mathrm{fast}} \times t) + A_2 \times \exp(-k_{\mathrm{slow}} \times t) + B \quad (8)$$

For real-world locations:

$$\mathrm{DF}(i) = A_1 \times \exp\left(-k_{\mathrm{fast}}(T_i I_i) \times 1\ \mathrm{h}\right) + A_2 \times \exp\left(-k_{\mathrm{slow}}(T_i I_i) \times 1\ \mathrm{h}\right) + B$$

$$\mathrm{DF\_total}(t) = \prod_{i=1}^{n(t)} \mathrm{DF}(i)$$

$$\mathrm{CE}(t) = \mathrm{CE}_0 \times \mathrm{DF\_total}(t) \quad (9)$$

T_i and I_i represents the temperature and light-intensity at hour i.

Since the degradation rate in the reference study was measured under constant illumination of 1200 W m^{-2}, we rescale the degradation rate at other light-intensity levels using the acceleration factor (AF)[35] defined as:

$$\mathrm{AF} = \frac{I_{\mathrm{acc}}}{I_{\mathrm{ref}}} \quad (10)$$

where I_{ref} is the reference light intensity (1200 W m^{-2}), and I_{acc} is the actual light intensity at a given hour. Although the present study focuses on degradation in J_{SC} *via* a reduction in CE, the modelling framework is sufficiently flexible to account for degradation arising from variations in other diode parameters.

2.4. Validation of modelling capabilities

This section demonstrates that EYcalc accurately reproduces the expected degradation trends and magnitudes under accelerated tests, thereby establishing confidence in its modelling capabilities. We use these cases as they provide clear expectations for directionality and scaling, which is necessary before applying the framework to complex, real-world operating conditions.

For model validation, we examine the impact of constant and cycled stressors for (i) temperature-induced and (ii) combined temperature- and light-induced degradation on the CE of the perovskite top cell and the overall performance of the PST solar cell.

2.4.1. Temperature-induced degradation. To examine the impact of temperature-induced degradation on the CE of the perovskite top cell and the overall performance of the PST solar cell, we vary the thermal stress. Since the reference case study[56] reported degradation rates under a constant illumination, parameters (*i.e.* k_0) exclusively linked to temperature-induced degradation (rather than light induced) cannot be extracted independently. To illustrate temperature-only behaviour, we scale k_0 one order of magnitude below the reference. To accurately quantify the impact of temperature-induced degradation, a dataset measured under dark conditions and controlled strictly for thermal variables would be required.

Examining the impact of different constant solar cell temperatures (65, 85, and 105 °C) on the CE of the perovskite top cell and the overall performance of the tandem solar cell reveals a more pronounced decline in the aggregated power ratio of the tandem solar cell at higher temperatures, as expected (Fig. 2, top row). Aggregated power ratio is defined as the ratio of the aggregated power output of the degraded cell to that of the non-degraded cell (see eqn (11)). Where $\mathrm{PR_{Agg}}$ is the aggregated power ratio, $P_{\mathrm{deg}}(t)$ is the cumulative power output of the degraded cell, $P_{\mathrm{ref}}(t)$ is the cumulative power output of the non-degraded cell, and N is the total number of hours considered.

$$\mathrm{PR_{Agg}}(t) = \frac{\sum_{t=1}^{N} P_{\mathrm{deg}}(t)}{\sum_{t=1}^{N} P_{\mathrm{ref}}(t)} \quad (11)$$

To enable a fair comparison between accelerated-test and real-world operation, where power output varies hourly, the aggregated power ratio is used in this study for both accelerated tests and real-world locations in the next sections. Investigating two cyclic cell temperature profiles (different duty cycles: short and long), with the same minimum (65 °C) and maximum (105 °C) temperatures and total duration as the constant-temperature cases, shows less degradation impact on the CE of the perovskite top cell and tandem solar cell performance than constant temperature exposure (Fig. 2, middle row). After 2000 hours, the device degrades approximately the same under constant exposure to 85 °C, and under a short-cycle temperature profile (3.6% *vs.* 3.7%). Although the short cycle peaks at 105 °C, higher than

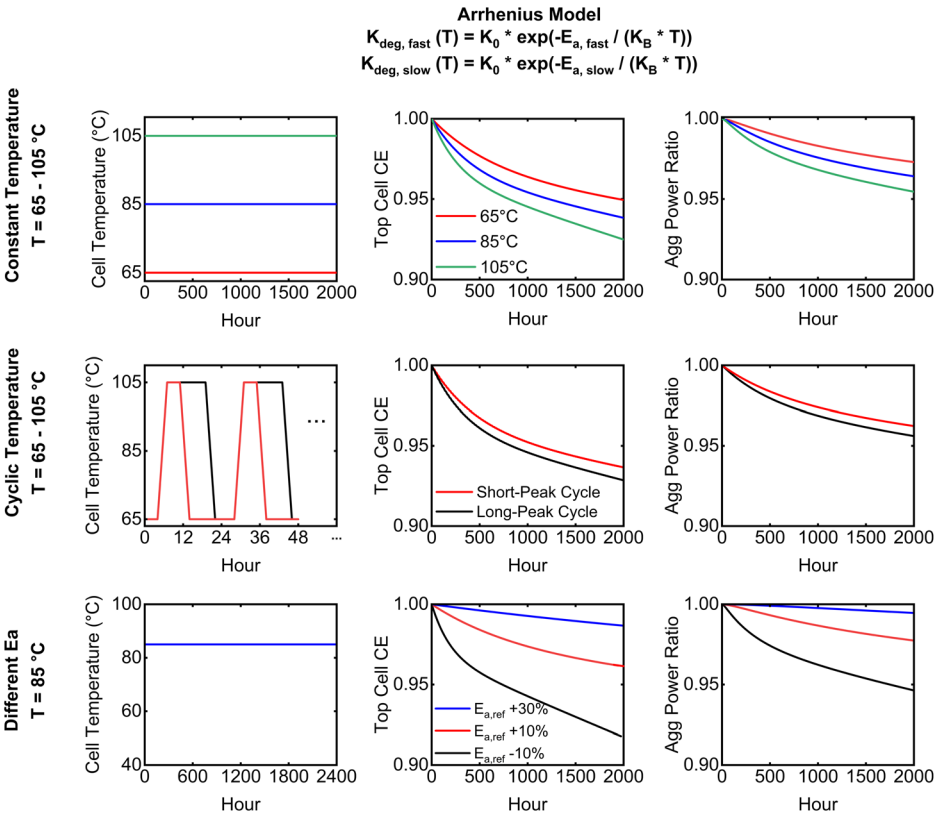

Fig. 2 Illustration of temperature-induced degradation impacting the collection efficiency (CE) of the perovskite top cell and the aggregated power ratio (Agg Power Ratio), defined as the ratio of the aggregated power output of the degraded cell to that of the non-degraded cell. Top row: Constant temperature conditions (65 °C, 85 °C, 105 °C) illustrating accelerated degradation with increasing thermal stress. Middle row: Cyclic temperature profiles with varying peak durations (short, long), representative of typical winter, and summer days. Bottom row: Effect of varying activation energy under constant temperature (85 °C).

the constant 85 °C, the degradation remains comparable. Thus, for the specific stress condition examined, where the cyclic temperature profile spans the same minimum–maximum range and total duration as the constant-temperature cases, the model predicts less degradation under cycling than under constant exposure. This result is presented simply as a consistency check for the model, rather than a general conclusion. Naturally, if the temperature bounds, duty cycles, or total duration of the cyclic profile were changed, the impact of degradation on the cell performance could vary, including cases where cycling stress may become more damaging than constant stress.

As shifts in activation energy change the degradation trends, we examine the impact of different activation energies (90–130% of the reference) on the CE of the perovskite top cell and the tandem device performance (Fig. 2, bottom row). Both activation energies, $E_{a,fast}$ and $E_{a,slow}$, which represent the fast and slow degradation processes, are scaled equally.

As expected, a decrease in the activation energy reveals a higher decline in the aggregated power ratio of the tandem device. It indicates increasing the activation energy from 90% to 130% of the reference (a 40% change) yields an 5% difference in aggregated power ratio after 2000 hours (99.5% *vs.* 94.5%) and a 12% difference after one year (98% *vs.* 86%). See Fig. SI2 for instantaneous power ratio (P_t/P_0), for all scenarios shown in Fig. 2.

2.4.2. Combined temperature- and light-induced degradation. In real-world environments, solar cells are exposed to both thermal and light stress. To emulate these combined stress conditions under controlled laboratory settings and recapitulate how the combination of these two stress factors affects the stability and performance of the tandem solar cell, we examine the influence of different constant light intensities (0.4–1 Sun at a fixed cell temperature of 85 °C) on the CE of the perovskite top cell and the overall performance of the tandem device. A more pronounced decline in the aggregated power ratio is revealed at higher light intensities (Fig. 3, top row), as expected. After 2000 hours, the tandem device shows ~13% degradation under 1 Sun, approximately double the ~7% degradation seen at 0.4 Sun. To enable a fair comparison with the constant-illumination cases, two cyclic light-intensity profiles (different duty cycles: short and long) were chosen to sweep between 0.4 and 1 Sun, covering the same minimum and maximum light intensities and the same total duration. At a fixed cell temperature of 85 °C, we then assess their impact on the CE of the perovskite top cell and on the overall tandem device performance (Fig. 3, bottom row). Under these comparable conditions, our model predicts that devices under constant illumination degrade more than those exposed to these specific cyclic profiles. After 2000 hours, the tandem device's aggregated

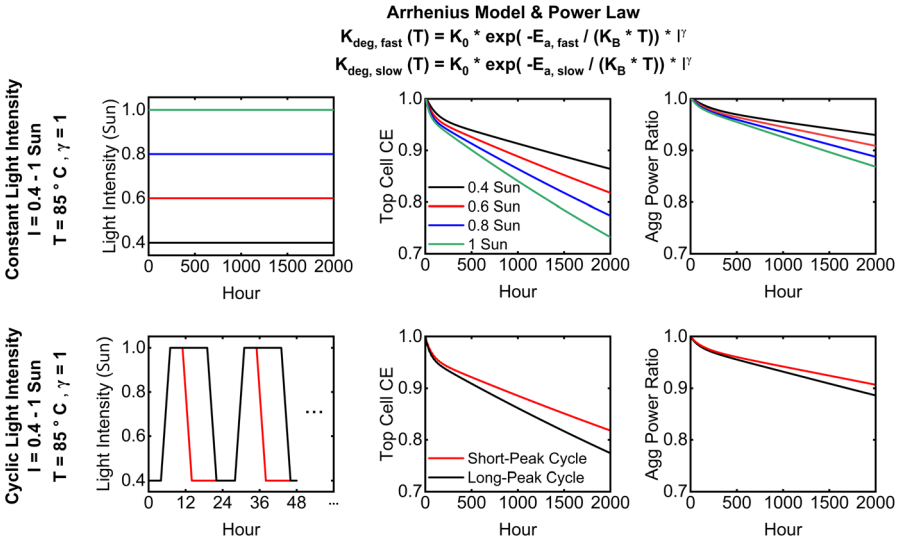

Fig. 3 Illustration of combined temperature- and light-induced degradation impacting the collection-efficiency (CE) of the perovskite top cell and the aggregated power ratio (Agg Power Ratio), defined as the ratio of the aggregated power output of the degraded cell to that of the non-degraded cell. All simulations assume a constant temperature of 85 °C. Top row: Constant light intensities (0.4–1 Sun) illustrating accelerated degradation with increasing light stress. Bottom row: Cyclic light intensity profiles with varying peak durations (short, long), representative of typical winter, and summer days demonstrating lower degradation rates compared to the constant illumination case.

power ratio drops by ~11.3% below the long cyclic profile which is similar to the decline witnessed under constant 0.8 Sun. Although the cyclic profile reaches peaks of 1 Sun, it still results in the same degradation to continuous exposure to 0.8 Sun. These examples are performed as consistency checks. If the light intensity bounds, duty cycles, or total duration of the cyclic profile change, the impact of degradation on the cell performance could shift, including cases where cycling stress become more detrimental than constant stress. By performing these consistency checks against accelerated test cases, the validation of the modelling capabilities confirms that the model reproduces degradation behaviour with expected trends and magnitudes. This demonstrates EYCalc suitability for application under more complex, real-world operating conditions, where the relationship between stressors and solar cell degradation is less apparent. See Fig. SI3 for instantaneous power ratio (P_t/P_0), for all scenarios shown in Fig. 3.

3. Results and discussions

Having validated the modelling capabilities of EYcalc in the Methodology section, we investigate how degradation trends observed under accelerated tests translate to degradation in real-world environments when solar cells are deployed to the field. Although accelerated tests provide valuable insights into the degradation of perovskite solar cells, their constant and controlled stress conditions fail to capture the real-world dynamic behaviour, such as temperature cycling, light cycling, and seasonal variations. Here, we highlight how the operational lifetime ($T_{90,Agg}$) of a PST solar cell exposed to temperature- and light-induced degradation substantially differs between typically performed accelerated tests and deployment to real-world operating conditions in numerous locations. As the stability of perovskite solar cells will improve in future, determining T_{80} may require increasingly long testing times. Also considering a benchmark annual degradation rate of 0.5%, a 20-year lifetime corresponds to approximately a 10% performance loss, which is close to T_{90}. Therefore, T_{90} is used in this study instead of the more commonly reported T_{80}. While T_{90} is conventionally defined using the instantaneous power ratio P_t/P_0, to enable a fair comparison between accelerated-test results and real-world operation, where power output varies on an hourly basis, the aggregated power ratio is used throughout this study. Accordingly, $T_{90,Agg}$ is defined as the time at which the aggregated power output of the degraded cell decreases to 90% of that of the non-degraded cell (see eqn (12)).

$$PR_{Agg}(T_{90,Agg}) = 0.9 \quad (12)$$

As detailed in the methodology, degradation in the tandem solar cell is assumed to arise from the perovskite top cell, while the performance of the silicon bottom cell remains unchanged in time. As degradation in solar cell parameters (J_{SC}, V_{OC}, FF) is analysed through variations in the corresponding diode parameters (CE, J_0, R_S, R_{Sh}), we evaluate the J_{SC} degradation in the perovskite top cell through variations in its CE. In this study, the degradation factor DF_total is therefore applied to CE rather than directly to PCE, representing degradation in the J_{SC}, and only this parameter is varied to isolate its contribution to the overall degradation (see methodology for more details). Accordingly, the degradation parameters used in the model (*e.g.*, k_0 and activation energies) are applied only to the perovskite top cell, while the silicon bottom cell parameters are kept constant. We parameterize degradation using the two activation energies reported for the reference device,[56] which represent

fast and slow processes (0.248 eV and 0.243 eV, respectively; see the methodology for details).

However, the framework is flexible and can be used for any device with any number of components. It can handle both simple cases with a single activation energy and more complex cases involving multiple processes. In this work, the degradation parameters used in the simulations are extracted from reported experimental data of the reference device experiencing degradation due to light-intensity and temperature.[56] Therefore, the model can predict the lifetime of any solar cell once the appropriate degradation parameters are provided. To validate this approach, the degradation of the reference device reported by Zhao *et al.*[56] was simulated using the extracted degradation parameters (Fig. SI8). The close agreement between simulated and experimental results confirms the capability of the model to predict the degradation lifetime of the device. In this work, we demonstrate how accelerated test results relate to real-world performance, quantify the impact of climate on operational lifetime across locations in the United States (U.S.), and convert ISOS-L2 (85 °C) lifetimes into field $T_{90,Agg}$ to identify the stability required for 10 years of use. First, a comparison between degradation trends observed in accelerated tests and degradation in two real-world locations highlights the difference between lifetimes estimated in laboratory tests and those observed under real-world conditions. Next, to explore the influence of climate variation on the lifetime of the tandem solar cell, we analyse the operational lifetime ($T_{90,Agg}$) across different locations in the U.S. Moreover, investigation of the relationship between operational lifetime and both cumulative light intensity and annual average cell temperature reveals which stressor primarily drives degradation of the PST solar cell. Finally, we investigate how $T_{90,Agg}$ values determined under ISOS-L2 (85 °C) testing conditions translate into corresponding $T_{90,Agg}$ predictions in real-world locations. This allows us to quantify the stability improvements required for the reference PST solar cell to reach a practical $T_{90,Agg}$ of 10 years under real-world conditions. We note that the results presented in this study reflect the degradation rates of the reference device used for parameterization. Although the framework is general and the degradation model predicts the lifetime of any solar cell in real-world locations based on controlled aging tests, direct cross-device comparisons are inappropriate because key degradation parameters in the degradation model (*e.g.*, Arrhenius pre-exponential factor k_0) are strongly materials- and architecture-dependent.

3.1. From accelerated tests to real-world conditions

Comparing accelerated tests with field operation shows that lab-estimated operational lifetimes ($T_{90,Agg}$) diverge substantially from real-world values (as one would expect for accelerated testing). Examining the cell performance under two different controlled aging tests (ISOS-L2 (85 °C) and a cyclic temperature and light profile) as well as two contrasting real-world locations (Phoenix (AZ) and Seattle (WA)) shows the impact of combined temperature- and light-induced degradation on the tandem solar cell performance and a significant difference between degradation under accelerated tests and in real-world locations (see Fig. 4).

Comparing the two controlled aging tests, we find that a cyclic test, selected to match the minimum and maximum temperatures and irradiances representative of Phoenix, leads to substantially less degradation than a constant-stress test such as ISOS-L2 (85 °C). We observe an approximately threefold decrease in the tandem solar cell aggregated power ratio under ISOS-L2 (85 °C) tests (43%) compared to the specific cyclic case (13%) after 1 year. Although the maximum temperature of the cyclic test does not reach ISOS-L2 (85 °C)'s constant 85 °C, such a gap in performance decline is not solely explained by temperature variation. Rather, it results from the fact that ISOS-L2 (85 °C) applies a continuous stress without interruption, whereas the cyclic test includes periods without stress, reflecting more realistic operating conditions.

Comparing the degradation during accelerated testing to degradation in real-world locations suggests that a cyclic aging test offers a more accurate prediction of degradation in real-world conditions. Investigating the degradation reveals a 43% annual decline in the aggregated power ratio of the tandem solar cell under ISOS-L2 (85 °C), whereas this value is only 13% and 5% for the cyclic aging test and Phoenix, respectively. This indicates that degradation under the ISOS-L2 (85 °C) test is ~9 times greater than that of real-world degradation in Phoenix, whereas it is only ~3 times greater in cyclic aging tests. Cyclic tests, which approximate real-world temperature and irradiance profiles, provide a more accurate estimate of degradation in real-world locations than constant stress tests, such as ISOS-L2 (85 °C). However, they still overestimate annual degradation compared to real-world observations. This discrepancy arises from seasonal variations (*e.g.*, cool winters and hot summers) as well as variation in daylight duration in real-world conditions, whereas the cyclic test applies a fixed cyclic profile that remains constant throughout the year.

Finally, comparing different locations highlights that climate affects degradation rates, as arid Phoenix shows greater annual loss than temperate Seattle. The higher cell temperatures and larger cumulative sun-hours in Phoenix result in a higher effective stress integral compared to Seattle, leading to a roughly two-percentage-point higher annual decline in aggregated power ratio in Phoenix.

3.2. Climate variation and lifetime of PST solar cell

To investigate the impact of climate variation on the operational lifetime ($T_{90,Agg}$) of a PST solar cell and evaluate the effect of temperature fluctuations against light-intensity variations, we compare six locations that span over a wide range of climatic zones: arid (Phoenix (AZ) and El Paso (TX)), temperate (Seattle (WA) and Portland (ME)), and tropical (Miami (FL) and Honolulu (HI)) (see Fig. 5). Our analysis reveals a substantial location- and climate-dependent variations in tandem solar cell operational lifetime. While the tandem solar cell exhibits a $T_{90,Agg}$ of approximately 2 months (~1440 h) based on the aggregated power ratio, its equivalent operational lifetime in real-world locations extends to dozens of months, depending on the

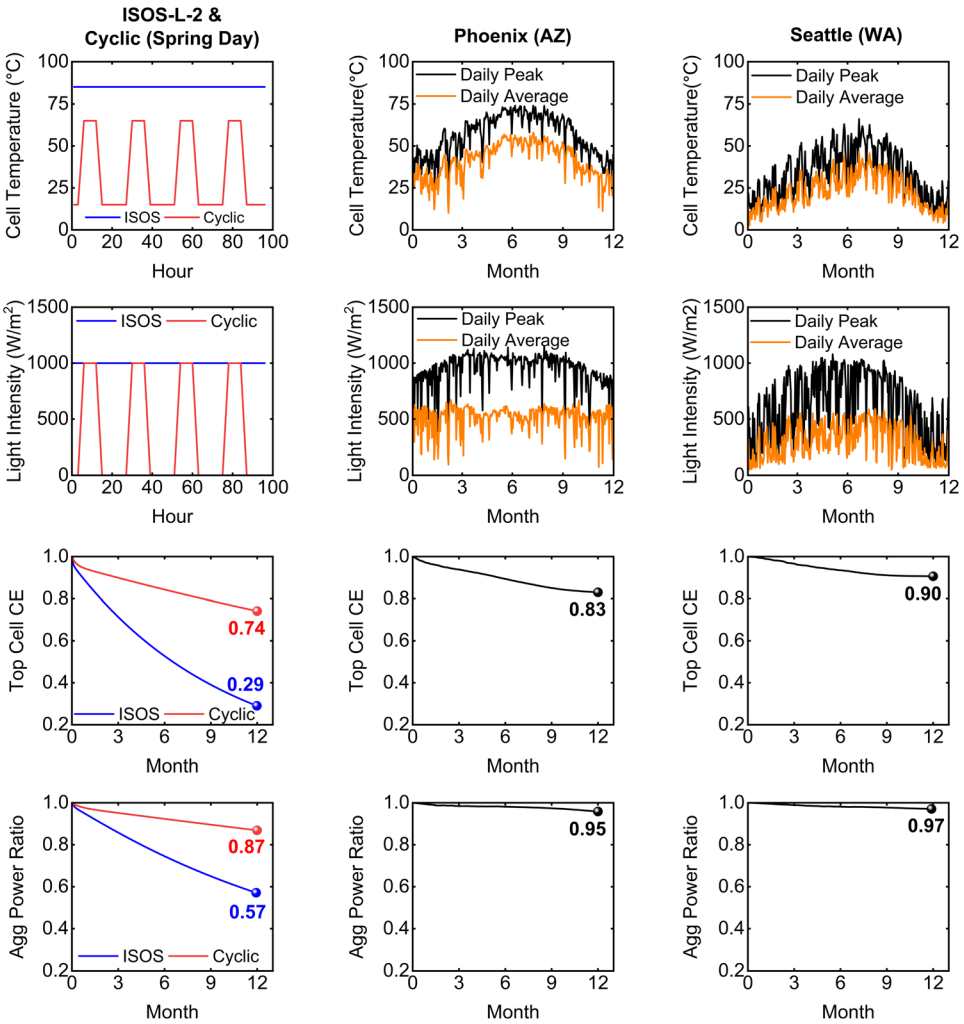

Fig. 4 Illustration of combined temperature-light-induced degradation impacting the collection efficiency (CE) of the perovskite top cell and the aggregated power ratio (Agg Power Ratio) of the tandem device under controlled laboratory conditions and real-world environments (aggregated power ratio is defined as the ratio of the aggregated power output of the degraded cell to that of the non-degraded cell). Controlled tests include the ISOS-L2 protocol and a cyclic light profile, both at a constant temperature of 85 °C. These are compared with outdoor exposure in two real-world locations (Phoenix (AZ) and Seattle (WA)), highlighting the differences between accelerated lab conditions and predictions for real-world operational stress.

local climatic conditions. Achieving around 30 months, arid locations have the shortest operational lifetimes, whereas temperate locations have the longest lifetimes of around 40 months.

This substantial difference is attributed to the severe climatic conditions (high temperatures and intense light) in arid locations, compared to the mild climatic conditions (mild temperatures and low light intensity) in temperate locations. Tropical locations exhibit a $T_{90,Agg}$ value somewhere between these two climates. Even within the same climate zone, operational lifetime varies as El Paso shows a $T_{90,Agg}$ of ~29 months *versus* Phoenix ~26 (arid), and Miami ~35 *versus* Honolulu ~32 (tropical).

Given that the solar cell under ISOS-L2 (85 °C) testing exhibits a 2-month lifetime, which translates to ~26 months in Phoenix and around 42 months in Seattle, this highlights the harsh degradation conditions of ISOS-L2 (85 °C), severely accelerating compared to real-world degradation.

Analysing the mapping between the $T_{90,Agg}$ of the solar cell and the average cell temperature and cumulative light intensity in each location highlights a linear relationship between the $T_{90,Agg}$ and cumulative annual light intensity. Locations with higher annual light intensity tend to degrade faster. In contrast, there is no similar linear relationship between $T_{90,Agg}$ and average cell temperature observable. For example, while the cell operates at higher temperatures in Honolulu than in El Paso, still longer $T_{90,Agg}$ is found for Honolulu compared to El Paso. This is because degradation rate is treated as exponentially increasing with temperature, thus maximum temperature is more important than the average temperature. Hourly temperature data (Fig. SI4) reveal that Honolulu's stable climate (minimal seasonal variation) results in a higher average temperature, whereas El Paso has colder winters (and thus

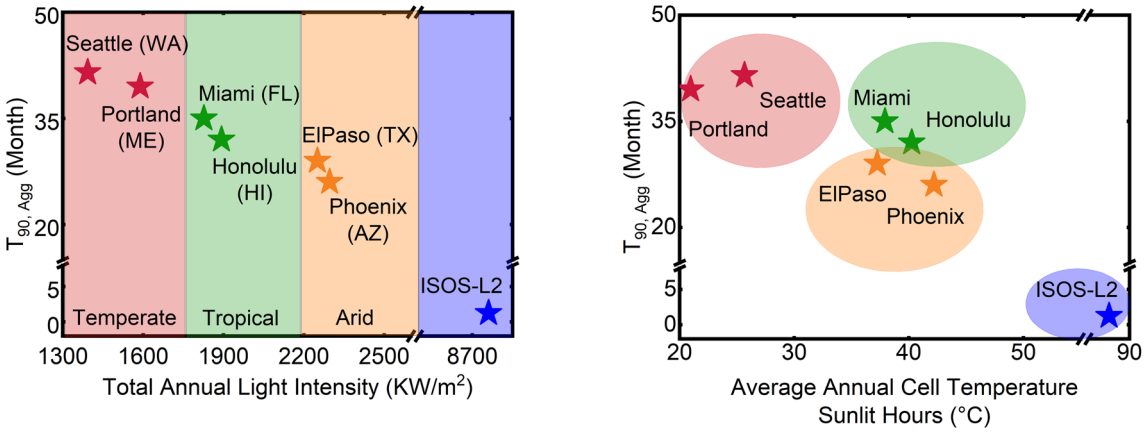

Fig. 5 Correlation between the operational lifetime ($T_{90,Agg}$) of a PST solar cell and (a) total annual light intensity and (b) average annual cell temperature during sunlit hours across six locations compared to ISOS-L2 (85 °C) (1 Sun, 85 °C). $T_{90,Agg}$ is defined as the time at which the aggregated power output of the degraded cell decreases to 90% of that of the non-degraded cell.

a lower average temperature) but summer temperatures that exceed those in Honolulu by 5–10 °C, leading to overall faster degradation. This finding highlights that seasonal variation plays a significant role in the degradation of solar cells and underlines why real-world condition modelling is required to predict the lifetime of the solar cells in the real world.

To investigate whether temperature fluctuations or light-intensity variations have a greater impact on the lifetime of a tandem solar cell, two distinct cases are considered. First, to isolate the effect of light variation, we assume that all locations share the same cell temperature as Phoenix, thereby removing the influence of temperature differences. Second, to isolate the effect of temperature variation, we assume that all locations share the same light intensity as Phoenix, while maintaining their original cell temperatures (see Fig. SI5). We find that temperature variation has a stronger influence on $T_{90,Agg}$ than light-intensity variation; the fixed-temperature case shows only slight variations in $T_{90,Agg}$ across all locations while the variations in $T_{90,Agg}$ are more pronounced in the fixed-irradiance case. This is expected as degradation is modelled as exponentially related to temperature, whereas irradiance is sub-linearly related.

A comparison of operational lifetimes in Seattle and Portland (see Fig. 5) reveals that the sunlight duration in different locations affects the lifetime of the tandem solar cell. Although Seattle experiences lower light intensity and higher cell temperatures than Portland, it is expected that Seattle would exhibit a shorter lifetime, as temperature fluctuations have been found to have a stronger impact on lifetime. However, the opposite is observed due to the difference in daylight duration between different locations, which is another important factor. While Seattle has a daylight duration of 3900 hours, Portland has a daylight duration of 4500 hours, exposing Portland to combined temperature and light stress for 600 hours longer. While it should be noted that real devices often exhibit night-time recovery, which our model omits, and degradation accumulates only during daylight, this finding highlights another important factor in real-world degradation that is ignored under standard accelerated tests.

3.3. Required accelerated test lifetime to reach outdoor stability

Having demonstrated a substantial difference in predicted tandem solar cell lifetime ($T_{90,Agg}$) under accelerated tests (*e.g.*, ISOS-L2 (85 °C)) and real-world conditions, we can likewise apply our model to investigate what lifetime under ISOS-L2 (85 °C) is required to ensure an acceptable operational lifetime in real-world locations.

To determine the lifetime needed under ISOS-L2 (85 °C) to produce an equivalent real-world lifetime, we explore how varying ISOS-L2 (85 °C) $T_{90,Agg}$ (1000, 2000, 4000, 6000, and 8000 hours), obtained by variation in the activation energy, translates to real-world $T_{90,Agg}$ values (see Fig. 6). Investigating the mapping for arid Phoenix (AZ), temperate Seattle (WA), and tropical Honolulu (HI) reveals considerable climate-dependent differences. Seattle, characterized by its mild temperature and moderate light intensity, achieves the longest operational lifetime across all tested conditions. In contrast, Phoenix, due to its extreme temperatures and light intensity, exhibits the shortest operational lifetime under every scenario. Honolulu displays intermediate behaviour, with lifetimes falling between those observed in Seattle and Phoenix. The findings indicate that ISOS-L2 (85 °C) $T_{90,Agg}$ values of 1000–2000 hours fall significantly short of delivering the operational lifetimes required for commercial use. A $T_{90,Agg}$ of 1000 hours under ISOS-L2 (85 °C) translates to an operational lifetime of approximately 1.5 years in Phoenix, 1.9 years in Honolulu, and 2.65 years in Seattle. Even if the ISOS-L2 (85 °C) $T_{90,Agg}$ is extended to 2000 hours, the real-world lifetimes only increase to roughly 2.9, 3.5, and 4.3 years in Phoenix, Honolulu, and Seattle, respectively. In response to this finding, we determine the required ISOS-L2 (85 °C) $T_{90,Agg}$ which corresponds to the operational lifetime of ~5 years across all studied real-world locations. It is found that a minimum $T_{90,Agg}$ of 4000 hours under ISOS-L2 (85 °C) is

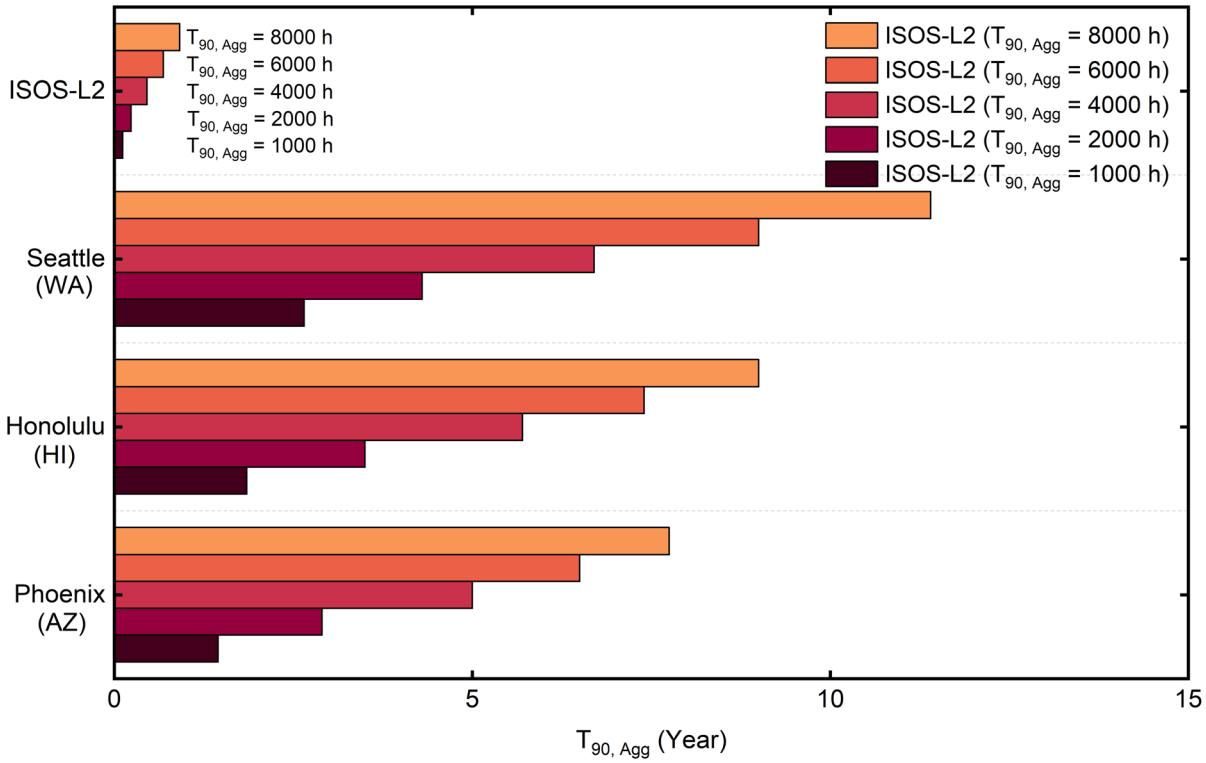

Fig. 6 $T_{90,Agg}$ values at different locations across the USA for ISOS-L2 (85 °C) reference lifetimes of 1000, 2000, 4000, 6000, 8000 hours. $T_{90,Agg}$ is defined as the time at which the aggregated power output of the degraded cell decreases to 90% of that of the non-degraded cell.

required to achieve an operational lifetime of more than 5 years in the investigated locations, resulting in a $T_{90,Agg}$ of approximately 5 years in Phoenix, 5.7 years in Honolulu and 6.7 years in Seattle. This finding indicates that a fourfold increase in ISOS-L2 (85 °C) $T_{90,Agg}$, compared to the benchmark 1000 hours, is necessary to guarantee at least a 5-year operational lifetime in a location with a harsh climate such as Phoenix.

Our mapping reveals that a $T_{90,Agg}$ of approximately 8000 hours under ISOS-L2 (85 °C) testing is required to achieve a lifetime of 10 years in a mild climate such as Seattle. However, for locations with harsher conditions, such as Phoenix and Honolulu, this duration is still insufficient, as a $T_{90,Agg}$ of 8000 hours under ISOS-L2 (85 °C) translates to an operational lifetime of only about 8 years in Phoenix and approximately 9 years in Honolulu.

These gaps between required $T_{90,Agg}$ under ISOS-L2 (85 °C) and practically achieved lifetimes imply substantial stability improvements are still required to ensure a 10-year operational lifetime across all locations. Relative to the reference cell's ISOS-L2 (85 °C) $T_{90,Agg}$ of 1440 h, achieving a 5-year lifetime across all locations requires an 3-fold increase (approx. 4000 h), while a 10-year lifetime in Seattle demands at least a sixfold increase in the ISOS-L2 (85 °C) $T_{90,Agg}$. As mentioned earlier, this study uses the aggregated power ratio and $T_{90,Agg}$ to enable a fair comparison between accelerated tests and real-world locations where power output fluctuates due to diurnal and seasonal variations. Given that T_{90} is conventionally defined based on the instantaneous power ratio (P_t/P_0), Fig. SI7 illustrates how identical instantaneous T_{90} values of 1000, 2000, 4000, 6000, and 8000 hours under ISOS-L2 (85 °C) translate into aggregated real-world lifetimes, across different locations. There we illustrate an instantaneous T_{90} of 8000 hours under ISOS-L2 (85 °C) corresponds to a $T_{90,Agg}$ of 20 years in Seattle, while the same condition does not reach 20 years in Phoenix and Honolulu. Attributing all $T_{90,Agg}$ variation to changes in activation energy, the required improvements are reflected by reduced temperature sensitivity of the device. For the investigated use case, a relative increase of at least 21% in the activation energy compared to the reference values is required to guarantee a 10-year lifetime in a mild real-world location like Seattle and an increase in activation energy of more than 13% suffices for at least 5 years across all studied locations (Fig. SI6). These results underline the critical need to enhance the intrinsic thermal stability of perovskite solar cells to achieve long-term operational reliability of PSTs across different climate conditions.

These findings are specific to the reference device and the modelled degradation mechanism, which assumes that variations arise solely from changes in activation energy. Modification to the device architecture may result in different behaviour, since the activation energy, pre-exponential factor (k_0), and the degradation mechanism may change (see ref. 56 for a comparison between devices with and without a 2D capping layer, and refer to the methodology). Although the results here focus on a single mechanism, EYCalc can be parameterized to simulate multiple, simultaneous degradation processes.

4. Conclusions

This work introduces a novel degradation function for EY modelling that translates trends from accelerated tests to real-world operations, enabling operational lifetime predictions for PST solar cells across diverse geographic locations and climates. We quantify the impact of combined temperature- and light-induced degradation on device performance, revealing large, climate-dependent gaps between lifetimes inferred from accelerated tests and those realized in the field. Applied to a published device, an ISOS-L2 (85 °C) $T_{90,Agg}$ of approximately two months (~1440 hours), due to photogenerated current density degradation, translates to several months outdoors, *e.g.*, 42 months in temperate Seattle (WA) and 26 months in arid Phoenix (AZ), underscoring strong climate dependence. Investigating the average cell temperature and cumulative light intensity reveals a linear dependence of the solar cell's $T_{90,Agg}$ on cumulative light, whereas dependence on temperature is more complex and exerts its influence mainly through variability and extremes rather than the annual average. Isolating stressors confirms that fluctuations in cell temperature have a stronger influence on the tandem solar cell's lifetime than variations in light intensity. Furthermore, we find that a minimum ISOS-L2 (85 °C) $T_{90,Agg}$ of 4000 hours is required to achieve a 5-year operational lifetime across diverse climates, whereas 8000 hours suffice for a 10-year lifetime in temperate climates, with harsher environments demanding even greater stability. These findings reflect kinetics fitted to the reference device and a single dominant degradation mechanism in which variations in $T_{90,Agg}$ are attributed solely to changes in activation energy, reflecting reduced temperature sensitivity of degradation. While requiring device-specific parameterization from appropriate aging tests, this approach is device agnostic, as the proposed degradation function is broadly applicable to different solar cell architectures and can be parameterized to simulate multiple degradation processes.

Author contributions

Seyedamir Orooji: conceptualization, data curation, formal analysis, investigation, methodology, software, visualization, writing – original draft. Felix Laufer: writing – review & editing. Sam Teale: writing – review & editing, Henry Snaith: writing – review & editing, Ulrich W. Paetzold: supervision, conceptualization, validation, writing – review & editing.

Conflicts of interest

There are no conflicts to declare.

Data availability

The data supporting the findings of this study, including complementary figures, and additional scenarios are available within the article and its supplementary information (SI). Supplementary information is available. See DOI: https://doi.org/10.1039/d6el00021e.

Acknowledgements

Funded by the European Union; views and opinions expressed are however those of the authors only and do not necessarily reflect those of the European Union or CINEA; neither the European Union nor the granting authority can be held responsible for them. NEXUS project has received funding from Horizon Europe Research and Innovation Action program under Grant Agreement no 101075330. The authors gratefully acknowledge financial support by the Helmholtz Association (project Zeitenwende, Solar Technology Acceleration Platform (Solar TAP), program-oriented funding period IV of the Helmholtz Association (Materials and Technologies for the Energy Transition, Topic 1: Photovoltaics and Wind Energy, Code: 38.01.02, the project EYCalcPlus)), and the Karlsruhe School of Optics and Photonics (KSOP).

References

1 N. R. E. Laboratory, Best Research-Cell Efficiency Chart, https://www.nrel.gov/pv/cell-efficiency.html, (accessed October, 2025).
2 E. B. V. Shaw, LONGi achieves 34.85% efficiency for two-terminal tandem perovskite solar cell, https://www.pv-magazine.com/2025/04/18/longi-achieves-34-85-efficiency-for-two-terminal-tandem-perovskite-solar-cell/, (accessed October, 2025).
3 L. G. E. Technology, Silicon-perovskite tandem solar cells — new world efficiency., https://www.longi.com/en/news/silicon-perovskite-tandem-solar-cells-new-world-efficiency/, (accessed October, 2025).
4 T. Niewelt, B. Steinhauser, A. Richter, B. Veith-Wolf, A. Fell, B. Hammann, N. E. Grant, L. Black, J. Tan, A. Youssef, J. D. Murphy, J. Schmidt, M. C. Schubert and S. W. Glunz, *Sol. Energy Mater. Sol. Cells*, 2022, **235**, 111467.
5 C. European Commission: Joint Research, *PV Status Report 2018*, Publications Office, 2018.
6 P.-J. Ribeyron, *Nat. Energy*, 2017, **2**, 17067.
7 Y. Li, B. Shi, Q. Xu, L. Yan, N. Ren, Y. Chen, W. Han, Q. Huang, Y. Zhao and X. Zhang, *Adv. Energy Mater.*, 2021, **11**, 2102046.
8 M. A. Green, A. Ho-Baillie and H. J. Snaith, *Nat. Photonics*, 2014, **8**, 506–514.
9 F. Schackmar, H. Eggers, M. Frericks, B. S. Richards, U. Lemmer, G. Hernandez-Sosa and U. W. Paetzold, *Adv. Mater. Technol.*, 2021, **6**, 2000271.
10 J. Roger, L. K. Schorn, M. Heydarian, A. Farag, T. Feeney, D. Baumann, H. Hu, F. Laufer, W. Duan, K. Ding, A. Lambertz, P. Fassl, M. Worgull and U. W. Paetzold, *Adv. Energy Mater.*, 2022, **12**, 2200961.
11 G. Yang, M. Wang, C. Fei, H. Gu, Z. J. Yu, A. Alasfour, Z. C. Holman and J. Huang, *ACS Energy Lett.*, 2023, **8**, 1639–1644.
12 G. Grancini, C. Roldán-Carmona, I. Zimmermann, E. Mosconi, X. Lee, D. Martineau, S. Narbey, F. Oswald, F. De Angelis, M. Graetzel and M. K. Nazeeruddin, *Nat. Commun.*, 2017, **8**, 15684.

13 R. Singh, H. Hu, T. Feeney, A. Diercks, F. Laufer, Y. Li, T. Duong, F. Schackmar, B. A. Nejand and U. W. Paetzold, *ACS Appl. Mater. Interfaces*, 2024, **16**, 27450–27462.
14 J.-P. Correa-Baena, M. Saliba, T. Buonassisi, M. Grätzel, A. Abate, W. Tress and A. Hagfeldt, *Science*, 2017, **358**, 739–744.
15 D. Wang, M. Wright, N. K. Elumalai and A. Uddin, *Sol. Energy Mater. Sol. Cells*, 2016, **147**, 255–275.
16 Y. Kato, L. K. Ono, M. V. Lee, S. Wang, S. R. Raga and Y. Qi, *Adv. Mater. Interfaces*, 2015, **2**, 1500195.
17 J. A. Schwenzer, L. Rakocevic, R. Gehlhaar, T. Abzieher, S. Gharibzadeh, S. Moghadamzadeh, A. Quintilla, B. S. Richards, U. Lemmer and U. W. Paetzold, *ACS Appl. Mater. Interfaces*, 2018, **10**, 16390–16399.
18 D. Zhang, D. Li, Y. Hu, A. Mei and H. Han, *Commun. Mater.*, 2022, **3**, 58.
19 B. Chen, J. Song, X. Dai, Y. Liu, P. N. Rudd, X. Hong and J. Huang, *Adv. Mater.*, 2019, **31**, 1902413.
20 F. Matteocci, L. Cinà, E. Lamanna, S. Cacovich, G. Divitini, P. A. Midgley, C. Ducati and A. Di Carlo, *Nano Energy*, 2016, **30**, 162–172.
21 Q. Emery, M. Remec, G. Paramasivam, S. Janke, J. Dagar, C. Ulbrich, R. Schlatmann, B. Stannowski, E. Unger and M. Khenkin, *ACS Appl. Mater. Interfaces*, 2022, **14**, 5159–5167.
22 R. Cheacharoen, C. C. Boyd, G. F. Burkhard, T. Leijtens, J. A. Raiford, K. A. Bush, S. F. Bent and M. D. McGehee, *Sustain. Energy Fuels*, 2018, **2**, 2398–2406.
23 Y. Cheng and L. Ding, *Energy Environ. Sci.*, 2021, **14**, 3233–3255.
24 A. F. Akbulatov, S. Y. Luchkin, L. A. Frolova, N. N. Dremova, K. L. Gerasimov, I. S. Zhidkov, D. V. Anokhin, E. Z. Kurmaev, K. J. Stevenson and P. A. Troshin, *J. Phys. Chem. Lett.*, 2017, **8**, 1211–1218.
25 J. Zhao, Y. Deng, H. Wei, X. Zheng, Z. Yu, Y. Shao, J. E. Shield and J. Huang, *Sci. Adv.*, 2017, **3**, eaao5616.
26 M. V. Khenkin, E. A. Katz, A. Abate, G. Bardizza, J. J. Berry, C. Brabec, F. Brunetti, V. Bulović, Q. Burlingame, A. Di Carlo, R. Cheacharoen, Y.-B. Cheng, A. Colsmann, S. Cros, K. Domanski, M. Dusza, C. J. Fell, S. R. Forrest, Y. Galagan, D. Di Girolamo, M. Grätzel, A. Hagfeldt, E. von Hauff, H. Hoppe, J. Kettle, H. Köbler, M. S. Leite, S. Liu, Y.-L. Loo, J. M. Luther, C.-Q. Ma, M. Madsen, M. Manceau, M. Matheron, M. McGehee, R. Meitzner, M. K. Nazeeruddin, A. F. Nogueira, Ç. Odabaşı, A. Osherov, N.-G. Park, M. O. Reese, F. De Rossi, M. Saliba, U. S. Schubert, H. J. Snaith, S. D. Stranks, W. Tress, P. A. Troshin, V. Turkovic, S. Veenstra, I. Visoly-Fisher, A. Walsh, T. Watson, H. Xie, R. Yıldırım, S. M. Zakeeruddin, K. Zhu and M. Lira-Cantu, *Nat. Energy*, 2020, **5**, 35–49.
27 FLUXiM, ISOS protocols: Stability of perovskite solar cells, https://www.fluxim.com/research-blogs/isos-protocols-stability-perovskite-solar-cells (accessed October, 2025).
28 R. Schmager, M. Langenhorst, F. Gota and J. Lehr, EYcalc – Energy yield calculator for multi-junction solar modules with realistic irradiance data and textured interfaces, *Zenodo*, 2021, DOI: 10.5281/zenodo.4696257.
29 D. B. Khadka, Y. Shirai, M. Yanagida, K. Uto and K. Miyano, *Sol. Energy Mater. Sol. Cells*, 2022, **246**, 111899.
30 A. Mavlonov, Y. Hishikawa, Y. Kawano, T. Negami, A. Hayakawa, S. Tsujimura, T. Okumura and T. Minemoto, *Sol. Energy Mater. Sol. Cells*, 2024, **277**, 113148.
31 Z. Zhang, H. Wang, T. J. Jacobsson and J. Luo, *Nat. Commun.*, 2022, **13**, 7639.
32 Y. Zhao, J. Zhang, Z. Xu, S. Sun, S. Langner, N. T. P. Hartono, T. Heumueller, Y. Hou, J. Elia, N. Li, G. J. Matt, X. Du, W. Meng, A. Osvet, K. Zhang, T. Stubhan, Y. Feng, J. Hauch, E. H. Sargent, T. Buonassisi and C. J. Brabec, *Nat. Commun.*, 2021, **12**, 2191.
33 U. M. Damo, C. G. Ozoegwu, C. Ogbonnaya and C. Maduabuchi, *Sol. Energy*, 2023, **250**, 335–346.
34 T. D. Siegler, W. A. Dunlap-Shohl, Y. Meng, Y. Yang, W. F. Kau, P. P. Sunkari, C. E. Tsai, Z. J. Armstrong, Y.-C. Chen, D. A. C. Beck, M. Meilă and H. W. Hillhouse, *J. Am. Chem. Soc.*, 2022, **144**, 5552–5561.
35 H. Zhu, S. Teale, M. N. Lintangpradipto, S. Mahesh, B. Chen, M. D. McGehee, E. H. Sargent and O. M. Bakr, *Nat. Rev. Mater.*, 2023, **8**, 569–586.
36 R. Schmager, M. Langenhorst, J. Lehr, U. Lemmer, B. S. Richards and U. W. Paetzold, *Opt. Express*, 2019, **27**, A507–A523.
37 S. Wilcox and W. Marion, *Users Manual for TMY3 Data Sets, Report NREL/TP-581-43156*, National Renewable Energy Laboratory, Golden, CO, USA, 2008.
38 C. C. C. S. (C3S), ERA5 reanalysis – single levels, https://cds.climate.copernicus.eu/cdsapp#!/dataset/reanalysis-era5-single-levels, (accessed October, 2025).
39 H. Hersbach, B. Bell, P. Berrisford, S. Hirahara, A. Horányi, J. Muñoz-Sabater, J. Nicolas, C. Peubey, R. Radu, D. Schepers, A. Simmons, C. Soci, S. Abdalla, X. Abellan, G. Balsamo, P. Bechtold, G. Biavati, J. Bidlot, M. Bonavita, G. De Chiara, P. Dahlgren, D. Dee, M. Diamantakis, R. Dragani, J. Flemming, R. Forbes, M. Fuentes, A. Geer, L. Haimberger, S. Healy, R. J. Hogan, E. Hólm, M. Janisková, S. Keeley, P. Laloyaux, P. Lopez, C. Lupu, G. Radnoti, P. de Rosnay, I. Rozum, F. Vamborg, S. Villaume and J.-N. Thépaut, *Q. J. R. Metereol. Soc.*, 2020, **146**, 1999–2049.
40 A. Inness, M. Ades, A. Agustí-Panareda, J. Barré, A. Benedictow, A. M. Blechschmidt, J. J. Dominguez, R. Engelen, H. Eskes, J. Flemming, V. Huijnen, L. Jones, Z. Kipling, S. Massart, M. Parrington, V. H. Peuch, M. Razinger, S. Remy, M. Schulz and M. Suttie, *Atmos. Chem. Phys.*, 2019, **19**, 3515–3556.
41 C. A. M. S. (CAMS), CAMS Global Reanalysis (EAC4), https://ads.atmosphere.copernicus.eu/cdsapp#!/dataset/cams-global-reanalysis-eac4.
42 C. A. Gueymard, *Sol. Energy*, 2001, **71**, 325–346.
43 S. C. Baker-Finch and K. R. McIntosh, *Prog. Photovoltaics Res. Appl.*, 2011, **19**, 406–416.
44 F. Gota, S. X. An, H. Hu, B. Abdollahi Nejand and U. W. Paetzold, *Adv. Opt. Mater.*, 2023, **11**, 2201691.
45 F. Gota, R. Schmager, A. Farag and U. W. Paetzold, *Opt. Express*, 2022, **30**, 14172–14188.

46 F. Gota, M. Langenhorst, R. Schmager, J. Lehr and U. Paetzold, *Joule*, 2020, **4**, 2387–2403.
47 M. De Bastiani, A. J. Mirabelli, Y. Hou, F. Gota, E. Aydin, T. G. Allen, J. Troughton, A. S. Subbiah, F. H. Isikgor, J. Liu, L. Xu, B. Chen, E. Van Kerschaver, D. Baran, B. Fraboni, M. F. Salvador, U. W. Paetzold, E. H. Sargent and S. De Wolf, *Nat. Energy*, 2021, **6**, 167–175.
48 Analog Devices, *LTspice [Computer software]*, Analog Devices, Inc., Wilmington, MA, USA, 2024, https://www.analog.com/en/resources/design-tools-and-calculators/ltspice-simulator.html, accessed April 2026.
49 M. C. Alonso García and J. L. Balenzategui, *Renewable Energy*, 2004, **29**, 1997–2010.
50 S. Orooji and U. W. Paetzold, *Energy Technol.*, 2024, **12**, 2400998.
51 M. V. Khenkin, A. K. M, I. Visoly-Fisher, S. Kolusheva, Y. Galagan, F. Di Giacomo, O. Vukovic, B. R. Patil, G. Sherafatipour, V. Turkovic, H.-G. Rubahn, M. Madsen, A. V. Mazanik and E. A. Katz, *ACS Appl. Energy Mater.*, 2018, **1**, 799–806.
52 M. Prete, M. V. Khenkin, D. Glowienka, B. R. Patil, J. S. Lissau, I. Dogan, J. L. Hansen, T. Leißner, J. Fiutowski, H. G. Rubahn, B. Julsgaard, P. Balling, V. Turkovic, Y. Galagan, E. A. Katz and M. Madsen, *ACS Appl. Energy Mater.*, 2021, **4**, 6562–6573.
53 T. Tayagaki, H. Kobayashi, K. Yamamoto, T. N. Murakami and M. Yoshita, *Sol. Energy Mater. Sol. Cells*, 2023, **263**, 112583.
54 G. Wenson, H. Thakkar, H. Tsai, J. Stein, R. Singh and W. Nie, *J. Mater. Chem. A*, 2022, **10**, 13519–13526.
55 J. Liu, Y. He, L. Ding, H. Zhang, Q. Li, L. Jia, J. Yu, T. W. Lau, M. Li, Y. Qin, X. Gu, F. Zhang, Q. Li, Y. Yang, S. Zhao, X. Wu, J. Liu, T. Liu, Y. Gao, Y. Wang, X. Dong, H. Chen, P. Li, T. Zhou, M. Yang, X. Ru, F. Peng, S. Yin, M. Qu, D. Zhao, Z. Zhao, M. Li, P. Guo, H. Yan, C. Xiao, P. Xiao, J. Yin, X. Zhang, Z. Li, B. He and X. Xu, *Nature*, 2024, **635**, 596–603.
56 X. Zhao, T. Liu, Q. C. Burlingame, T. Liu, R. Holley, G. Cheng, N. Yao, F. Gao and Y.-L. Loo, *Science*, 2022, **377**, 307–310.